THE UNIVERSITY OF MICHIGAN
INDUSTRY PROGRAM OF THE COLLEGE OF ENGINEERING

WAKE OF A CHARGED PROLATE SPHERIOD AT ANGLE OF ATTACK IN A RAREFIED PLASMA

Walter Sawchuk

November, 1962

IP-590

CONTENTS

LIST OF FIGURES

I

INTRODUCTION

This report deals with the theoretical problem of satellite interaction with a rarefied or collision-free plasma. The specific objective of this study is to determine the wake produced by a conducting prolate-spheroid moving in the ionosphere at a speed intermediate to electron and ion thermal speeds. Because the object is not spherically symmetric, the significance of angle of attack on the flow field characteristics is considered. The earth's magnetic field is neglected in all calculations.

Previous workers (1, 2, 3, 4) in the field have, in general, considered objects of small size (less than a Debye length) which allowed them to emphasize electro- and magneto-hydrodynamics over ordinary hydrodynamical phenomena. Large size objects have received less attention due to the great complexity of the problem. References 5 and 6 are examples of studies of flow fields associated with large objects. In the present discussion, only steady state conditions in such flow fields are considered; therefore, time dependent plasma phenomena are neglected. It will be assumed that the ion flow can be obtained by neglecting the effect of the satellite electrostatic force field on the ions, i.e., the ion wake results mainly from the shadowing effect produced by the satellite.

It is assumed that the electrons are always in equilibrium in the potential

field surrounding the satellite; i.e. due to their mobility, they adjust themselves to the ion distribution, the potential on the satellite surface, and zero potential at infinity. As mentioned previously, this is a steady state approach and does not treat other phenomena such as electron plasma oscillations, ion waves, Alfvén waves, etc. The electron density is obtained from a solution of Poisson's equation, and is a quasi-self-consistent approach in which a constraint is placed on the ion density.

For the electron equilibrium conditions to be valid, it has to be assumed that the satellite surface has little influence upon the Maxwellian distribution for the electrons. Due to the present lack of knowledge concerning particle-surface interactions, especially charged particles, for want of a better model it will be assumed that particles reflected diffusely or specularly from the satellite are neutralized near or at the satellite surface. Consequently, re-emitted particles need not be considered since only the behavior of ionized particles is of interest here.

During final preparation of this report some algebraic and geometric errors were discovered. These errors affected all cases except $\alpha=0^{o}$ and 90^{o}, hence the data presented here for $\alpha=45^{o}$ are quantitatively in error. It is believed that the data are qualitatively correct and therefore can be considered as representative of near wake conditions at that flight attitude. The far wake flow field configuration depicted is believed to approximate closely the correct solution since it is less sensitive to body orientation.

II

BASIC EQUATIONS

1. Formulation of Problem

For a highly rarefied plasma in which both binary and Fokker-Planck (grazing) type of collisions are neglected, the problem of describing the characteristics of the flow field surrounding a charged body moving in a weakly ionized plasma may be formulated in terms of the collision-free Boltzmann equations, namely,

$$\frac{\partial f_e}{\partial t} + \vec{V}' \cdot \vec{\nabla} f_e + (e/m) \vec{\nabla} \phi \cdot \vec{\nabla}_v f_e = 0, \tag{1}$$

$$\frac{\partial f_i}{\partial t} + \vec{V}' \cdot \vec{\nabla} f_i - (e/M) \vec{\nabla} \phi \cdot \vec{\nabla}_v f_i = 0, \tag{2}$$

and Poisson's equation,

$$\nabla^2 \phi = (e/\epsilon_0)\left[\int f_e \, d\vec{V}' - \int f_i \, d\vec{V}'\right], \tag{3}$$

where,

e = electron charge,

m = electron mass,

M = ion mass,

f_e = electron distribution function

f_i = ion distribution function,

$\vec{V}'$ = total velocity of gas particle

n_o = ambient electron or ion density,

ϕ = potential field,

θ = kT = ion or electron ambient temperature,

ϵ_o = dielectric constant of free space

Under present assumptions that the satellite speed is intermediate to that of the positive ions and the electrons and that the electrons are in equilibrium at all times, the satellite appears to be at rest with respect to the electrons and the electron distribution function will be Maxwellian in the resulting potential field, that is,

$$f_e = n_o \left(\frac{m}{2\pi\theta}\right)^{3/2} e^{\left(e\phi - \frac{mV'^2}{2}\right)\Big/\theta}. \tag{4}$$

The corresponding electron density is

$$n_e = n_o e^{e\phi/\theta}. \tag{5}$$

As far as the positive ions are concerned, the problem is much more difficult to solve. Formally the ion distribution may be written as

$$f_i(\vec{r}, \vec{v}, t) = f_1(\vec{r}, \vec{v}) + f_2(\vec{r}, \vec{v}, t), \tag{6}$$

where $f_1(\vec{r}, \vec{v})$ denotes a steady state condition. At large distances from the satellite, equation (6) may be written as

$$f_i(\vec{r}, \vec{v}, t) = f_o(\vec{r}, \vec{v}) + f'(\vec{r}, \vec{v}) + f_2(\vec{r}, \vec{v}, t), \tag{7}$$

with f_o Maxwellian and f' a small perturbation. In this region $f_2(\vec{r}, \vec{v}, t)$ is

also a small perturbation and accounts for collective ionic oscillations. This aspect of the problem was treated by Yoshihara (2) based on the work of Kraus and Watson (1).

While $f_1(\vec{r}, \vec{v})$ in equation (6) can be used directly to deduce ion densities, the same result can be obtained without actually specifying this function. (See reference 5.) That is, by ignoring the influence of the electrostatic field on the ions, the ion density can then be defined as

$$n_i = \int_{\infty} f_i \, d\vec{v} = \int_{*} f_o \, d\vec{v} \, . \tag{8}$$

The asterisk on the integral sign denotes that integration over velocity space is subject to conditions on the velocity vectors. Specifically, in the present case, it is necessary to exclude all particles that fall within the shadow cone from the point of interest to the spheroid.

2. Ion Distribution

Determination of the positive ion flow is based on the kinetic theory method used by Dolph and Weil (5) to solve the flow field problem for the motion of a sphere in a dilute gas. This method is now extended to the case of a conducting prolate spheroid moving in an ionized medium with uniform velocity, U', and with an angle of attack, α, which is restricted to the X-Z plane. This mathematical simplification introduces no limitation to the scope of the problem when the ambient

atmosphere is quiescent. The presence of appreciable atmospheric streaming velocities would necessitate a modification of the problem to include side-slip. Both the angle of attack and eccentricity of the spheroid are arbitrary. The resulting ion density distribution can also be considered to be an estimate of the electron density, since charge separation is constrained by the presence of coulomb forces.

For convenience, $\vec{U}'$ and $\vec{V}'$ are normalized with respect to ionic thermal speeds, namely,

$$\vec{v} = \vec{V}' \Big/ \sqrt{2kT/M} = \vec{V}' \Big/ \sqrt{2\theta/M} \tag{9}$$

$$\vec{u} = \vec{U}' \Big/ \sqrt{2kT/M} = \vec{U}' \Big/ \sqrt{2\theta/M} \ .$$

The ion distribution function, equation (8), is considered to be Maxwellian. Hence, using a reference system in which the satellite is at rest in a uniform stream having a velocity $\vec{U}'$, the ion distribution is given as

$$f_o = n_o \left(\frac{M}{2\pi\theta}\right)^{3/2} e^{-|\vec{v} - \vec{u}|^2} \ , \tag{10}$$

and the density at points of interest in space is

$$n_i = n_o \left(\frac{1}{\pi}\right)^{3/2} \int_* e^{-|\vec{v} - \vec{u}|^2} \, dv_x \, dv_y \, dv_z \ . \tag{11}$$

The geometrical configuration used in formulating the present problem is shown in Figure 1. At any point $P(X_1, Y_1, Z_1)$ equation (11) is to be integrated over velocity space excluding velocities which characterize particles within the

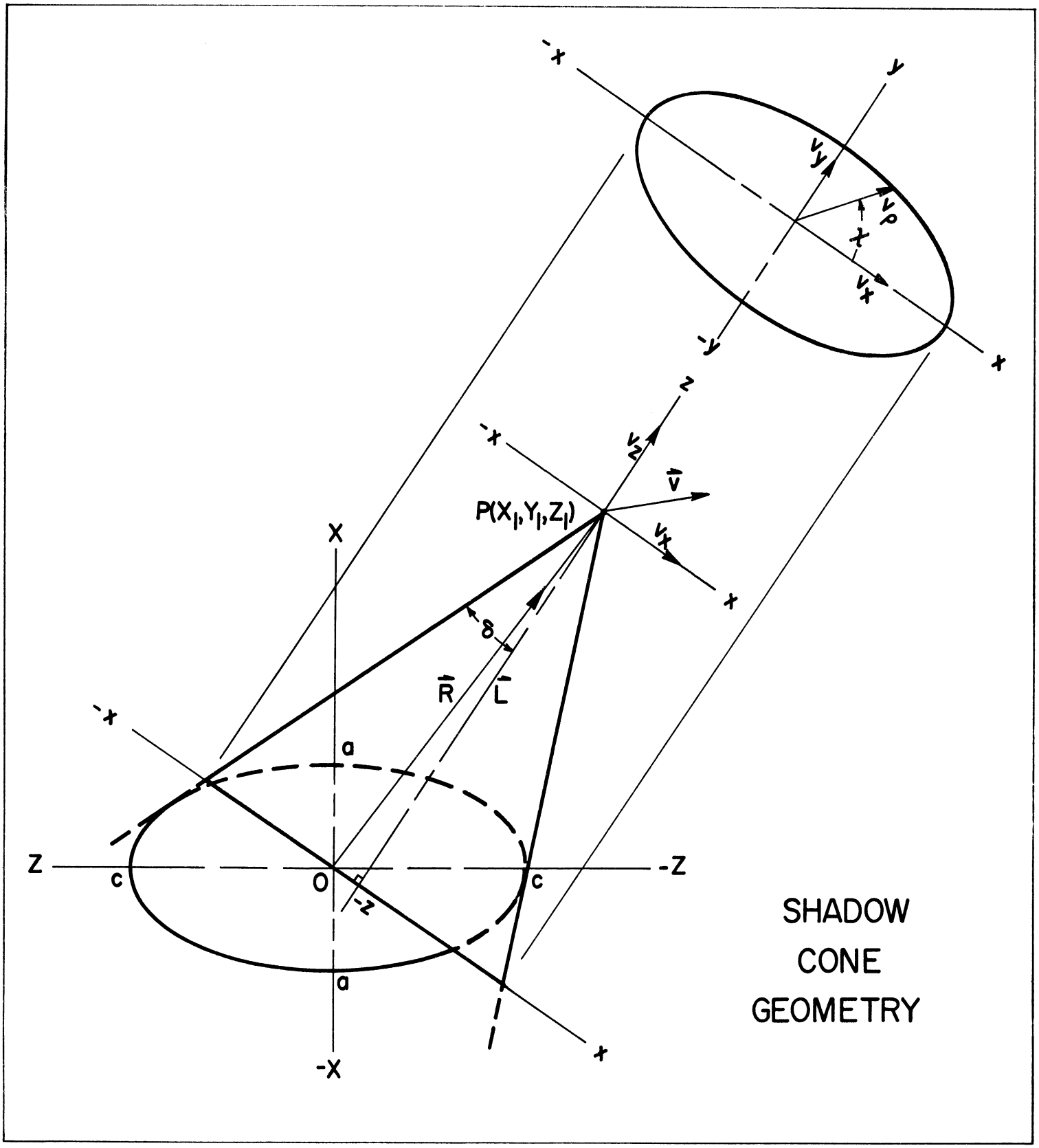
-x
y
v_y
v_p
x
v_x
-y
x
z
-x
v_z
$\vec{v}$
$P(X_1, Y_1, Z_1)$
v_x
x
X
δ
$\vec{R}$
$\vec{L}$
-x
a
Z
c
O
c
-Z
-z
a
-X
x
SHADOW
CONE
GEOMETRY

Figure 1.

shadow cone from P to the spheroid. Unfortunately, unlike the case of the sphere, the shadow cone is not symmetrical about the position vector R; hence, it is necessary to align the coordinate system, whose origin is at P, in such a manner that the z axis is colinear with the principal axis of the cone from point P to the spheroid. Writing the equation of the spheroid as

$$\frac{X^2 + Y^2}{a^2} + \frac{Z^2}{c^2} = 1, \tag{12}$$

the equation of the tangential cone becomes

$$\left[\frac{X_1^2 + Y_1^2}{a^2} + \frac{Z_1^2}{c^2} - 1\right]\left[\frac{X^2 + Y^2}{a^2} + \frac{Z^2}{c^2} - 1\right] - \left[\frac{XX_1 + YY_1}{a^2} + \frac{ZZ_1}{c^2} - 1\right]^2 = 0 \tag{13}$$

We now translate coordinates to (X_1, Y_1, Z_1) and obtain the shadow cone in the new coordinate system by setting $X = X_1 + x'$, $Y = Y_1 + y'$, and $Z = Z_1 + z'$. This yields

$$Ax'^2 + By'^2 + Cz'^2 + 2Fx'y' + 2Gx'z' + Hy'z' = 0. \tag{14}$$

The coefficients in explicit form are as follows:

$$A = \left[\frac{X_1^2}{a^2} + \frac{Y_1^2}{a^2} - 1\right] \tag{a}$$

$$B = \left[\frac{Y_1^2}{a^2} + \frac{Z_1^2}{c^2} - 1\right] \tag{b}$$

$$C = \left[\frac{X_1^2}{a^2} + \frac{Z_1^2}{c^2} - 1\right] \tag{c}$$

$$F = -X_1 Y_1 / a^4 \qquad \text{(d)}$$

$$G = -X_1 Z_1 / a^2 c^2 \qquad \text{(e)} \qquad (15)$$

$$H = -Y_1 Z_1 / a^2 c^2 \qquad \text{(f)}$$

The next step is to rotate the new coordinate system about point P to establish colinearity with the principal axis of the cone. Points of configuration space in this coordinate system are denoted by (x, y, z).

Equation (14) may be written in matrix form as

$$(x', y', z') \begin{pmatrix} A & F & G \\ F & B & H \\ G & H & C \end{pmatrix} \begin{pmatrix} x' \\ y' \\ z' \end{pmatrix} = 0, \qquad (16)$$

and the eigenvalues are obtained by solving the determinant of the corresponding secular equation, namely,

$$\begin{vmatrix} (A-\lambda) & F & G \\ F & (B-\lambda) & H \\ G & H & (C-\lambda) \end{vmatrix} = 0. \qquad (17a)$$

or

$$\lambda^3 - (A+B+C)\lambda^2 + (AB+AC+BC-F^2-G^2-H^2)\lambda - (ABC+2FGH-AH^2 - BG^2 - CF^2) = 0 \qquad (17b)$$

The roots of equation (17b) are denoted by d_1, d_2, and $-d_3$. The direction cosines corresponding to the total transformation are obtained from solutions of

$$\begin{pmatrix} A & F & G \\ F & B & H \\ G & H & C \end{pmatrix} \begin{pmatrix} \alpha_{11} \\ \alpha_{21} \\ \alpha_{31} \end{pmatrix} = d_1 \begin{pmatrix} \alpha_{11} \\ \alpha_{21} \\ \alpha_{31} \end{pmatrix}. \tag{18}$$

etc. The principal equation of the cone is then

$$d_1 x^2 + d_2 y^2 - d_3 z^2 = 0. \tag{19}$$

The actual formulas for the direction cosines and their coding as used in the problem are given in detail in Appendix A and Table I-A. With the above results taken into consideration, equation (11) may now be written as

$$n_i(X_1, Y_1, Z_1) = n_o \left(\frac{1}{\pi}\right)^{3/2} \int_* e^{-\left[(v_x - u_x)^2 + (v_y - u_y)^2 + (v_z - u_z)^2\right]} dv_x dv_y dv_z , \tag{20}$$

with

$$\begin{aligned} u_x &= (u \sin \alpha)\ \alpha_{11} + (u \cos \alpha)\ \alpha_{31} && \text{(a)} \\ u_y &= (u \sin \alpha)\ \alpha_{12} + (u \cos \alpha)\ \alpha_{32} && \text{(b)} \\ u_z &= (u \sin \alpha)\ \alpha_{13} + (u \cos \alpha)\ \alpha_{33} && \text{(c)} \end{aligned} \tag{21}$$

To exclude the particles within the shadow cone it is necessary that certain conditions be satisfied (5), namely,

$$\frac{v_z}{\sqrt{v_x^2 + v_y^2 + v_z^2}} \leq \cos\delta = \frac{|L|}{\sqrt{\rho^2 + L^2}} \tag{22}$$

Here, L is the height of the cone defined in such a way that the base passes through the origin of the original coordinate system (X, Y, Z) and ρ is the radius vector of the ellipse defined by the plane $z = -L$. The distance L is also equal to the projection of the position vector, $\vec{R}(X_1, Y_1, Z_1)$ on the principal axis (z axis) of the cone. Since the direction cosines of the latter are known, this gives

$$L = \alpha_{13} X_1 + \alpha_{23} Y_1 + \alpha_{33} Z_1 . \tag{23}$$

From equation (19), the equation of the elliptical base of the cone becomes

$$\frac{x^2}{\left(\frac{|d_3| L^2}{d_1}\right)} + \frac{y^2}{\left(\frac{|d_3| L^2}{d_2}\right)} = 1 . \tag{24}$$

Obviously the major and minor axes of the ellipse are $L\left(\frac{|d_3|}{d_1}\right)^{1/2}$ and $L\left(\frac{|d_3|}{d_2}\right)^{1/2}$ respectively; therefore, in terms of polar coordinates

$$\rho^2 = |d_3| L^2 \left[d_2 + (d_1 - d_2)\cos^2\chi\right]^{-1} , \tag{25}$$

where χ is always measured from the positive semi-major axis (x axis) of the base of the cone. The condition specified by equation (22) may now be written as

$$\xi = \frac{|L|}{\rho}\left(v_x^2 + v_y^2\right)^{1/2} = \frac{\left(v_x^2 + v_y^2\right)^{1/2}\left[d_2 + (d_1 - d_2)\cos^2\chi\right]^{1/2}}{\left(|d_3|\right)^{1/2}} \qquad (26)$$

where ξ equals the limiting value of v_z. Then equation (20) may be written as

$$n_i = n_o\left(\frac{1}{\pi}\right)^{3/2}\int_{-\infty}^{+\infty}\int_{-\infty}^{+\infty}\int_{-\infty}^{\xi} \exp\left[-\left\{(v_x-u_x)^2 + (v_y-u_y)^2 + (v_z-u_z)^2\right\}\right] dv_x dv_y dv_z. \qquad (27)$$

Integration over v_z can be carried out directly to yield

$$n_i = \frac{n_o}{2} + \frac{n_o}{2\pi}\int_{-\infty}^{+\infty}\int_{-\infty}^{+\infty} e^{-\left[(v_x-u_x)^2 + (v_y-u_y)^2\right]} \quad \mathbf{X}$$

$$\mathbf{X}\ \operatorname{erf}\left[\frac{|L|}{\rho}\left(v_x^2 + v_y^2\right)^{1/2} - u_z\right] dv_x dv_y. \qquad (28)$$

If the following mathematical transformations are now made (5),

$$\begin{aligned} v_x &= v_\rho \cos\chi & u_x &= \left(u^2 - u_z^2\right)^{1/2}\cos\psi \\ v_y &= v_\rho \sin\chi & u_y &= \left(u^2 - u_z^2\right)^{1/2}\sin\psi \end{aligned} \qquad (29)$$

equation (28) becomes

$$n_i = \frac{n_o}{2} + \frac{n_o}{2\pi} e^{-(u^2-u_z^2)} \int_0^{\infty} v_\rho e^{-v_\rho^2} dv_\rho \int_0^{2\pi} \exp\left[2 v_\rho (u^2-u_z^2)^{1/2} \cos(\chi - \psi)\right] \quad X$$

$$X \quad \operatorname{erf}\left[\frac{v_\rho \left[d_2 + (d_1 - d_2)\cos^2\chi\right]^{1/2}}{\left(|d_3|\right)^{1/2}} - u_z\right] d\chi \qquad (30)$$

which is also written in more convenient form for analysis as

$$n_i = n_o \left\{1 - \frac{e^{-(u^2-u_z^2)}}{2\pi} \int_0^{\infty} v_\rho e^{-v_\rho^2} dv_\rho \int_0^{2\pi} \exp\left[2v_\rho (u^2-u_z^2)^{1/2} \cos(\chi - \psi)\right] \quad X\right.$$

$$\left. X \quad \operatorname{erfc}\left[\frac{v_\rho \left[d_2 + (d_1 - d_2)\cos^2\chi\right]^{1/2}}{\left(|d_3|\right)^{1/2}} - u_z\right] d\chi \right\} \qquad (31)$$

Positive ion distributions in the wake are shown in Figures (2, 5, 8, 10, and 13). Equation (31) will be used as a source term in Poisson's equation; however, it is first necessary to determine the potential of the satellite.

Satellite Potential

For a particular angle of attack, the potential of the satellite will be constant; therefore, the total flux of ions and electrons to the surface must be equal. Since

an exact calculation of fluxes is extremely difficult, approximations must be used. The equation for the flux per unit area is

$$dF_i = \frac{n_o}{2\sqrt{\pi}} \left(\frac{2\theta}{M}\right)^{1/2} \left\{e^{-u^2} + \sqrt{\pi}\ u(1+\text{erf}\, u)\right\} . \tag{32}$$

The accretion of positive charge is due mainly to the "ram" effect of the ions over the frontal area of the satellite. Consequently, the total ion flux may be approximated by multiplying the flux per unit area by the cross-sectional area the satellite presents to the mean flow. The frontal area of the prolate spheroid at angle of attack, or the cross-sectional area of the enveloping stream tube, is derived in Appendix B. Hence, the total ion flux is

$$F_i = \frac{n_o}{2\sqrt{\pi}} \left(\frac{2\theta}{M}\right)^{1/2} \pi a^2 \left[3\cos^2\alpha + 1\right]^{1/2} \left[e^{-u^2} + \sqrt{\pi}\ u\,(1 + \text{erf}\, u)\right] \tag{33}$$

The total electron flux is calculated by considering the satellite to be at rest relative to the electrons, and using the equilibrium electron distribution function in the presence of the satellite potential field. The flux per unit area is then uniform over the satellite surface and is given by

$$dF_e = \frac{n_o}{2\sqrt{\pi}} \left(\frac{2\theta}{m}\right)^{1/2} e^{-e\phi_o/\theta} , \tag{34}$$

where ϕ_o is the surface potential of the satellite. The total flux is found by multiplying equation (34) by the total surface area of the satellite or,

$$F_e = \frac{n_o}{2\sqrt{\pi}} \left(\frac{2\theta}{m}\right)^{1/2} e^{-\phi_o/\theta} \left[2\pi a^2 + 4\pi a^2 \frac{\sin^{-1}\epsilon}{\epsilon}\right] \tag{35}$$

where $\epsilon = \frac{(c^2 - a^2)^{1/2}}{c}$, the eccentricity of the prolate spheroid.

Since $c = 2a$ in the present case

$$\epsilon = \frac{\sqrt{4a^2 - a^2}}{2a} = \frac{\sqrt{3}}{2} . \tag{36}$$

Equating equations (33) and (35) and taking the logarithm of both sides yields

$$\phi_o = \frac{\theta}{e} \log \left[\frac{2\,(M/m)^{1/2} \left(1 + 2\,\frac{\sin^{-1}\epsilon}{\epsilon}\right)}{\left(e^{-u^2} + \sqrt{\pi}\ \mathrm{erf}\ u\right) \sqrt{3\cos^2\alpha + 1}}\right] \tag{37}$$

For $u > 1$, equation (37) may be approximated by

$$\phi_o = \frac{\theta}{e} \log \left[\frac{(2\theta/m)^{1/2} \left(1 + 2\,\frac{\sin^{-1}\epsilon}{\epsilon}\right)}{\sqrt{\pi}\ u \sqrt{3\cos^2\alpha + 1}}\right] \tag{38}$$

4. Electron Density

Determination of the electron density distribution in the medium surrounding

the satellite and in the wake is obtained through the use of Poisson's equations, [equation (3)]. By rewriting this equation in the form

$$\nabla^2 \phi = \frac{\epsilon}{\epsilon_o} \left[n_e - n_i \right]$$

and substituting equations (5) and (31), Poisson's equation is expressed in terms of the parameters of the problem, namely,

$$\nabla^2 \phi = \frac{n_o e}{\epsilon_o} \left\{ e^{e\phi/\theta} + 1 + \frac{e^{-(u^2 - u_z^2)}}{2\pi} \int_0^{\infty} \int_0^{2\pi} v_\rho \, e^{-v_\rho^2} \exp\left[2 v_\rho \, (u^2 - u_z^2)^{\frac{1}{2}} \cos(\chi - \psi) \right] \mathrm{X} \right.$$

$$\left. \mathrm{X} \quad \operatorname{erfc}\left[\frac{v_\rho \left[d_2 + (d_1 - d_2) \cos^2 \chi \right]^{\frac{1}{2}}}{\left(|d_3| \right)^{\frac{1}{2}}} - u_z \right] dv_\rho \, d\chi \right\} \qquad (39)$$

Then using equation (38) and an iteration procedure, quasi-self-consistent solutions of equation (39) for the values of ϕ are obtained. Substitution of these values of ϕ into equation (5) give the corresponding values of the electron density, n_e. Electron density distributions in the wake are shown in Figures 3, 6, 9, 11, and 14.

III

NUMERICAL PROCEDURES FOR DETERMINING THE ELECTRON, ION, AND EQUIPOTENTIAL DISTRIBUTIONS

The numerical analysis utilized both IBM 709 and 7090 electronic computers. The programming was performed by the Computation Department of the Institute of Science and Technology, and this work is described in detail in a separate report (8). Only a brief summary will be given here.

The computational program falls naturally into two main parts: the determination of the ion densities as given by equation (31) and the electron densities from the solution of equation (39). Only normalized values of densities are of interest and are denoted by

$$g = n_i/n_o \quad \text{and} \quad h = n_e/n_o = e^{e\phi/\theta}. \tag{40}$$

In determining the g values, the characteristic cubic equation (17b) was solved numerically on the computer and the direction cosines obtained according to the formulas given in Appendix A. The double integral of equation (31) was evaluated using Simpson's rule. The limit 0 to ∞ was replaced by 0 to 4, the latter condition being determined by trial and error convergence tests of equation (31).

The second major phase of the program was the solution of Poisson's equation using the Gauss iterative procedure (9). The following formula was used:

$$\phi^{[N]}_{(\alpha,\beta,\gamma)} = \left[\frac{1}{h_1h_2} + \frac{1}{k_1k_2} + \frac{1}{l_1l_2}\right]^{-1}\left[\frac{\phi_{(\alpha+1,\beta,\gamma)}}{h_2(h_1+h_2)} + \frac{\phi_{(\alpha-1,\beta,\gamma)}}{h_1(h_1+h_2)} + \right.$$

$$+ \frac{\phi_{(\alpha_1,\beta+1,\gamma)}}{k_2(k_1+k_2)} + \frac{\phi_{(\alpha_1,\beta-1,\gamma)}}{k_1(k_1+k_2)} + \frac{\phi_{(\alpha_1,\beta,\gamma+1)}}{l_2(l_1+l_2)} + \frac{\phi_{(\alpha_1,\beta,\gamma-1)}}{l_1(l_1+l_2)} +$$

$$\left. + \frac{1}{2} A\left(e^{\frac{e\phi}{\theta}^{[N-1]}} - g_{(\alpha,\beta,\gamma)}\right)\right] . \qquad (41)$$

Here

N = Iteration number,

$\phi_{(\alpha,\beta,\gamma)}$ = Value of the potential at the point (α,β,γ),

A = $n_o e/\epsilon_o$,

h, k, ℓ = Distance from a mesh point to the adjacent mesh point or the boundary of the satellite, whichever is shorter, in the X, Y, Z direction.

$()_1$ = Measurement made in a positive direction.

$()_2$ = Measurement made in a negative direction.

$g_{(\alpha,\beta,\gamma)}$ = Value of g at the point (α,β,γ),

In performing the iteration process, the satellite and its flow field were considered to be enclosed in a rectangular box which was subdivided by a three-dimensional grid, the mesh size of which could be varied automatically. For all

angles of attack, the body centered axis (X, Y, Z) was used to orient the grid of the box and initial box dimensions were determined by the distances required for the ion densities to approach their ambient values. The value of the potential on all surfaces of the box was chosen to be zero. In order to double the number of mesh points near the satellite, the volume of the box was reduced, and the iteration process repeated. This procedure was adopted because of the limited core storage of the IBM 7090 computer.

Two such runs were made for each angle of attack. The initial lattice spacing was one meter and the latter one-half meter. The initial values of the potentials (ϕ^*) were such as to make the electron density equal to the ion density or

$$\phi^*_{(\alpha,\beta,\gamma)} = (\theta/e) \ln g_{(\alpha,\beta,\gamma)} \tag{42}$$

When data of the two runs were compared, good matching of the values of the potential was obtained in regions remote from the satellite, i.e., at distances greater than 3 c. This was not the case in the vicinity of the satellite where steep potential gradients demand that a much finer mesh be used due to rapid variation of the potential field. Since the present program was written for computer core storage, use of a finer mesh size would have exceeded its storage capacity. Conversion of the present program to utilize tape storage instead of core storage to obtain a much higher accuracy in the computation of electron densities is planned.

IV

CONCLUSION AND DISCUSSION

In the previous sections, the motion of a conducting prolate spheroid in a rarefied plasma was considered. Results of numerical calculations for a prolate spheroid having a major axis of 4 meters and a minor axis of 2 meters and moving at 8 km/sec at an altitude of 500 km have been plotted for angles of attack of 0^{o}, 45^{o}, and 90^{o}. At this height the ambient temperature and electron density are approximately 0.1 electron volts and $10^{6}/cm^{3}$, respectively.

The ion distribution, subject to the approximations used, was successively extended beyond the previous sphere case (5). The electron density was determined from an iterative solution of Poisson's equation and yields results which are more realistic than those obtained using the assumption of equal electron-ion densities in the wake. In the near wake the results for the electron density distribution are not as accurate as those in the far wake. This was due to the fact that the computer program was originally written to utilize core storage, the capacity of which was inadequate to accommodate the fine mesh needed to describe the larger gradients. The program is to be converted to tape storage.

The diagrams present separate plots for the positive ion and electron density distributions and for the net charge distribution in the wake for each angle of

attack. Figures 2 through 14 are enclosed at the end of the report. Figures 2, 3, and 4 refer to the zero angle of attack case. Figures 5, 6, 7, 8, and 9 represent the $\alpha = 45^{o}$ case. The first three figures are representations of major plane variations and the last two, of similar variations in the minor plane. Figures 10, 11, 12, 13, and 14 refer to the $\alpha = 90^{o}$ case and are arranged as in the $\alpha = 45^{o}$ case.*

Comparison of the drawings illustrates the dependence of wake length on the nature of the cross-sectional area the satellite presents to the mean flow. In addition, the depletion of both electron and ion densities immediately behind the satellite indicates a similar dependence. Due to their mobility, the electrons tend to fill in the wake cavity much more rapidly than the ions, and this accounts for the shallower gradients in their flow field. In the vicinity of the satellite, as previously mentioned, the mesh size was too large to give a proper representation of sheath thickness on the frontal region of the satellite. The fact that a sheath thickness greater than reality is calculated means that indicated gradients are shallower than they should be while total populations remain unchanged. Therefore, the accuracy of the electron density calculation could be improved by the use of a smaller mesh length. To emphasize this point, the flow lines around the front of the satellite have been omitted in the drawings. It should be noted that as the mesh size decreases, the flow field contour lines near the satellite will move

*See page 2 for explanatory note on $\alpha = 45^{o}$ case.

progressively closer to the body until the mesh size becomes the order of a Debye length.

The satellite potential for each angle of attack was determined on the basis of equal total ion and electron fluxes. The values of ϕ_o for the three angles of attack are listed below.

Angle of Attack (α)	Satellite Potential (ϕ_o) (volts)
0^o	-0.36
45^o	-0.33
90^o	-0.29

Since the total electron flux is constant and independent of angle of attack while for ions the frontal area is angle of attack dependent (the maximum occurring at 90^o), the negative potential will decrease in magnitude with increasing angle of attack. The calculated results are of the same order of magnitude as the experimental values given by Bourdeau, et al, (7) for a satellite which approximated the shape of an oblate spheroid. Since the existence of an electron shadowing effect would tend to reduce the total electron accretion on the surface, and since present results take into account neither the effect of the earth's magnetic

field nor the photo-electric effect, which would tend to lower the magnitude of the potentials, it appears that the results given here are reasonable for the level of approximation being used.

It should be noted that while equipotential contours have not been drawn, these are similar to those for the electron density, and their magnitude can be obtained from $\phi = (\theta/e) \log (n_e/n_o)$.

Figures 4, 7, and 12 illustrate the net charge distribution and show the plasma sheath characteristics in the wake. In general, the wake sheath consists of a negative inner core of conical shape surrounded by a positive layer. An interesting feature in the wake is the nature of the maximum negative density contours which are centered along the axis of mean flow for zero angle of attack but move off the axis at $\alpha = 90^o$ toward the top of the satellite and to an intermediate position at $\alpha = 45^o$.

Since satellites in general are not spherical, the results of the present work should provide a better understanding of the flow field associated with satellites and thereby permit a better evaluation of ionospheric measurements made aboard such vehicles. An extension of this work would include a study of the flow fields of prolate spheroids of large eccentricities, which approximate cylinders, as well as the effects of dielectric surfaces instead of perfect conductors. Refinement of

the iteration program to obtain results which may be used to investigate approximate methods of solution to reduce the time and effort required to attain satisfactory results is also contemplated.

ACKNOWLEDGEMENT

The author would like to acknowledge the assistance of Dr. Richard Leite and Dr. Conrad Mason of the Radiation Laboratory who read and reviewed the manuscript and suggested clarifications which were adopted in the report.

He would also like to acknowledge the help of Mr. O. Ruehr for his assistance with the geometrical aspects of the problem and would like to express his appreciation to Mr. D. B. Kirk, Associate Research Mathematician, and to Mr. R. S. Gould, Programmer of the Computation Department, Institute of Science and Technology, for invaluable assistance with the programming of the problem for IBM 709 - 7090 computers.

REFERENCES

1. Kraus, L. and K. M. Watson, 1958, Physics of Fluids 1, 480.

2. Yoshihara, H., 1961, Physics of Fluids 4, 100.

3. Pines, D. and D. Bohm, 1952, Phys. Rev. 85, 338.

4. Greifinger, P. S., 1961, Physics of Fluids 4, 194.

5. Dolph, C. L. and H. Weil, 1959, "Studies in Radar Cross Sections XXXVII—Enhancement of Radar Cross Sections of Warheads and Satellites by the Plasma Sheath," Radiation Laboratory Report No. 2778-2-F, The University of Michigan.

6. Gurevich, A. V., 1961, Iskustvennye Sputniki Zemli, (Artificial Earth Satellite), 7, 101.

7. Bourdeau, R. E., J. L. Donley, G. P. Serbu, and E. C. Whipple, 1961, "Measurements of Sheath Currents and Equilibrium Potential on the Explorer VIII Satellite," American Astronautical Society Symposium, Washington, D.C.

8. Gould, R. S. and D. B. Kirk, 1961, "WR43, WR44A, WR44B Satellite Program for IBM 709 - 7090 Computer," Computation Department, Institute of Science and Technology, The University of Michigan.

9. Nielson, K. L., 1956, Methods in Numerical Analysis, McMillan Company, New York.

APPENDIX A

EQUATIONS FOR DIRECTION COSINES

The cubic characteristic equation is solved numerically for the three roots, and the resulting eigenvalues are kept in the following form:

d_1 = the smaller positive root,

d_2 = the larger positive root,

d_3 = the single negative root.

The direction cosines are evaluated according to the following scheme:

A. For j = 1 and 3,

$$\alpha_{1j} = \frac{\left[FH - G(B - d_j)\right]}{\left\{\left[FH - G(B - d_j)\right]^2 + \left[FG - H(A - d_j)\right]^2 + \left[F^2 - (A - d_j)(B - d_j)\right]^2\right\}^{1/2}},$$

$$\alpha_{2j} = \frac{\left[FG - H(A - d_j)\right]}{\left\{\left[FG - H(A - d_j)\right]^2 + \left[FH - G(B - d_j)\right]^2 + \left[F^2 - (A - d_j)(B - d_j)\right]^2\right\}^{1/2}},$$

$$\alpha_{3j} = \frac{\left[F^2 - (A - d_j)(B - d_j)\right]}{\left\{\left[F^2 - (A - d_j)(B - d_j)\right]^2 + \left[FH - G(B - d_j)\right]^2 + \left[FG - H(A - d_j)\right]^2\right\}^{1/2}}.$$

For j = 2,

$$\alpha_{12} = \frac{F}{\left[(A - d_2)^2 + F^2\right]^{1/2}}; \quad \alpha_{22} = \frac{(A - d_2)}{\left[(A - d_2)^2 + F^2\right]^{1/2}}; \quad \alpha_{32} = 0.$$

B. Whenever the point of interest is on one of the coordinate planes, then

if $X = 0$,

$$\alpha_{11} = 0, \qquad \alpha_{21} = \frac{H}{\left[(B-d_1)^2+H^2\right]^{1/2}}, \qquad \alpha_{31} = \frac{(B-d_1)}{\left[(B-d_1)^2+H^2\right]^{1/2}},$$

$$\alpha_{12} = 1, \qquad \alpha_{22} = 0, \qquad \alpha_{32} = 0;$$

$$\alpha_{13} = 0, \qquad \alpha_{23} = \frac{H}{\left[(B-d_3)^2+H^2\right]^{1/2}}, \qquad \alpha_{33} = \frac{(B-d_3)}{\left[(B-d_3)^2+H^2\right]^{1/2}};$$

if $Y = 0$,

$$\alpha_{11} = \frac{G}{\left[G^2+(A-d_1)^2\right]^{1/2}}, \qquad \alpha_{21} = 0, \qquad \alpha_{31} = \frac{(A-d_1)}{\left[G^2+(A-d_1)^2\right]^{1/2}},$$

$$\alpha_{12} = 0, \qquad \alpha_{22} = 1, \qquad \alpha_{32} = 0,$$

$$\alpha_{13} = \frac{G}{\left[G^2+(A-d_3)^2\right]^{1/2}}, \qquad \alpha_{23} = 0, \qquad \alpha_{33} = \frac{(A-d_3)}{\left[G^2+(A-d_3)^2\right]^{1/2}};$$

and if $Z = 0$,

$$\alpha_{11} = 0, \qquad \alpha_{21} = 0, \qquad \alpha_{31} = 1,$$

$$\alpha_{12} = \frac{F}{\left[(A-d_2)^2+F^2\right]^{1/2}}, \qquad \alpha_{22} = \frac{(A-d_2)}{\left[(A-d_2)^2+F^2\right]^{1/2}}, \qquad \alpha_{32} = 0,$$

$$\alpha_{13} = \frac{F}{\left[(A-d_3)^2+F^2\right]^{1/2}}, \qquad \alpha_{23} = \frac{(A-d_3)}{\left[(A-d_3)^2+F^2\right]^{1/2}}, \qquad \alpha_{33} = 0.$$

The signs used are given in Table A-I. In this table a polarity sign alone indicates that the formulas in Appendix A are to be used. However, when a value such as zero or unity appears, this quantity is to be used directly without any additional equations.

TABLE A-I

Direction Cosine Polarity Coding

X_1	Y_1	Z_1	α_{11}	α_{21}	α_{31}	α_{12}	α_{22}	α_{32}	α_{13}	α_{23}	α_{33}
+	+	+	+	+	-	-	+	0	+	+	+
+	+	-	-	-	-	-	+	0	+	+	-
+	-	+	+	-	-	+	+	0	+	-	+
+	-	-	-	+	-	+	+	0	+	-	-
-	-	+	-	-	-	+	-	0	-	-	+
-	-	-	+	+	-	+	-	0	-	-	-
-	+	+	-	+	-	-	-	0	-	+	+
-	+	-	+	+	-	-	-	0	-	+	-
0	+	+	0	+	-	-1	0	0	0	+	+
0	+	-	0	-	-	-1	0	0	0	+	-
0	-	-	0	+	-	+1	0	0	0	-	-
0	-	+	0	-	-	+1	0	0	0	-	+

TABLE A-I (Concluded)

Direction Cosine Polarity Coding

X_1	Y_1	Z_1	α_{11}	α_{21}	α_{31}	α_{12}	α_{22}	α_{32}	α_{13}	α_{23}	α_{33}
+	+	0	0	0	-1	-	+	0	+	+	0
+	-	0	0	0	-1	+	+	0	+	-	0
-	-	0	0	0	-1	+	-	0	-	-	0
-	+	0	0	0	-1	-	-	0	-	+	0
+	0	+	+	0	-	0	+1	0	+	0	+
+	0	-	-	0	-	0	+1	0	+	0	-
-	0	-	+	0	-	0	-1	0	-	0	-
-	0	+	-	0	-	0	-1	0	-	0	+
0	0	+	+1	0	0	0	+1	0	0	0	+1
0	0	-	+1	0	0	0	-1	0	0	0	-1
+	0	0	0	0	-1	0	+1	0	+1	0	0
-	0	0	0	0	-1	0	-1	0	-1	0	0
0	+	0	0	0	-1	-1	0	0	0	+1	0
0	-	0	0	0	-1	+1	0	0	0	-1	0

APPENDIX B

FRONTAL AREA OF PROLATE SPHEROID AS FUNCTION OF ANGLE OF ATTACK

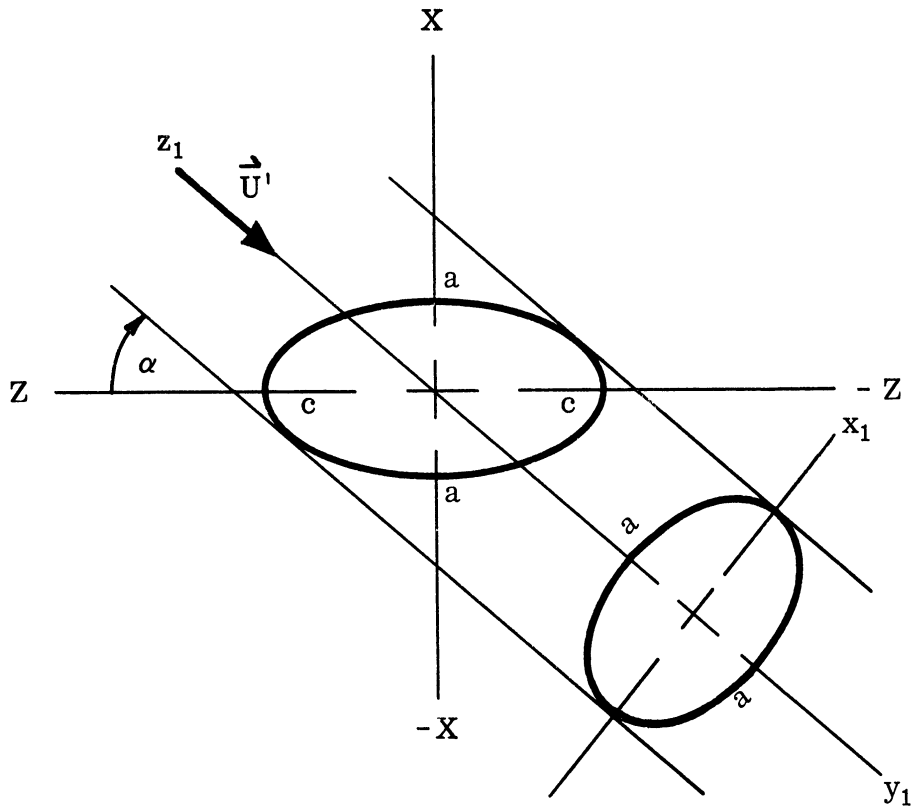

Figure B-1

The equation for the enveloping stream tube may be written as:

$$\left[\frac{X^2}{a^2}+\frac{Y^2}{a^2}+\frac{Z^2}{c^2}-1\right]\left[\frac{\ell^2}{a^2}+\frac{n^2}{c^2}\right]-\left[\frac{\ell X}{a^2}+\frac{nZ}{c^2}\right]^2=0\,. \qquad \text{(B-1)}$$

The enveloping stream tube is then oriented along the principal axis, namely,

$$Z = z_1 \cos\alpha - x_1 \sin\alpha = z_1 n - x_1 \ell$$
$$X = z_1 \sin\alpha + x_1 \cos\alpha = z_1 \ell + x_1 n \qquad \text{(B-2)}$$

To get the cross-sectional area of the ellipse we merely set $z_1 = 0$, which then yields an equation for the ellipse of the form.

$$x_1^2 \left[\left(\frac{n^2}{a^2} + \frac{\ell^2}{c^2} \right) - \ell^2 n^2 \frac{\left(\frac{1}{a^2} - \frac{1}{c^2} \right)^2}{\left(\frac{\ell^2}{a^2} + \frac{n^2}{c^2} \right)} \right] + \frac{y_1^2}{a^2} = 1 \qquad \text{(B-3)}$$

If we set $c = 2a$, according to our specific problems, equation (B-3) becomes

$$\frac{x_1^2}{a^2 (4\ell^2 + n^2)} + \frac{y_1^2}{a^2} = 1 \ . \qquad \text{(B-4)}$$

One notes that

if $\alpha = 0$, then $x_1^2 + y_1^2 = a^2$, a circle;

and

if $\alpha = 90^\circ$, then $\left(\frac{x_1^2}{4a^2} + \frac{y_1^2}{a^2} \right) = 1$, an ellipse. $\qquad \text{(B-5)}$

Expressed in terms of angle of attack (α), the frontal area intercepted by the cylindrical stream tube is given by

$$A = \pi a^2 (3 \sin^2\alpha + 1)^{1/2} \ . \qquad \text{(B-6)}$$

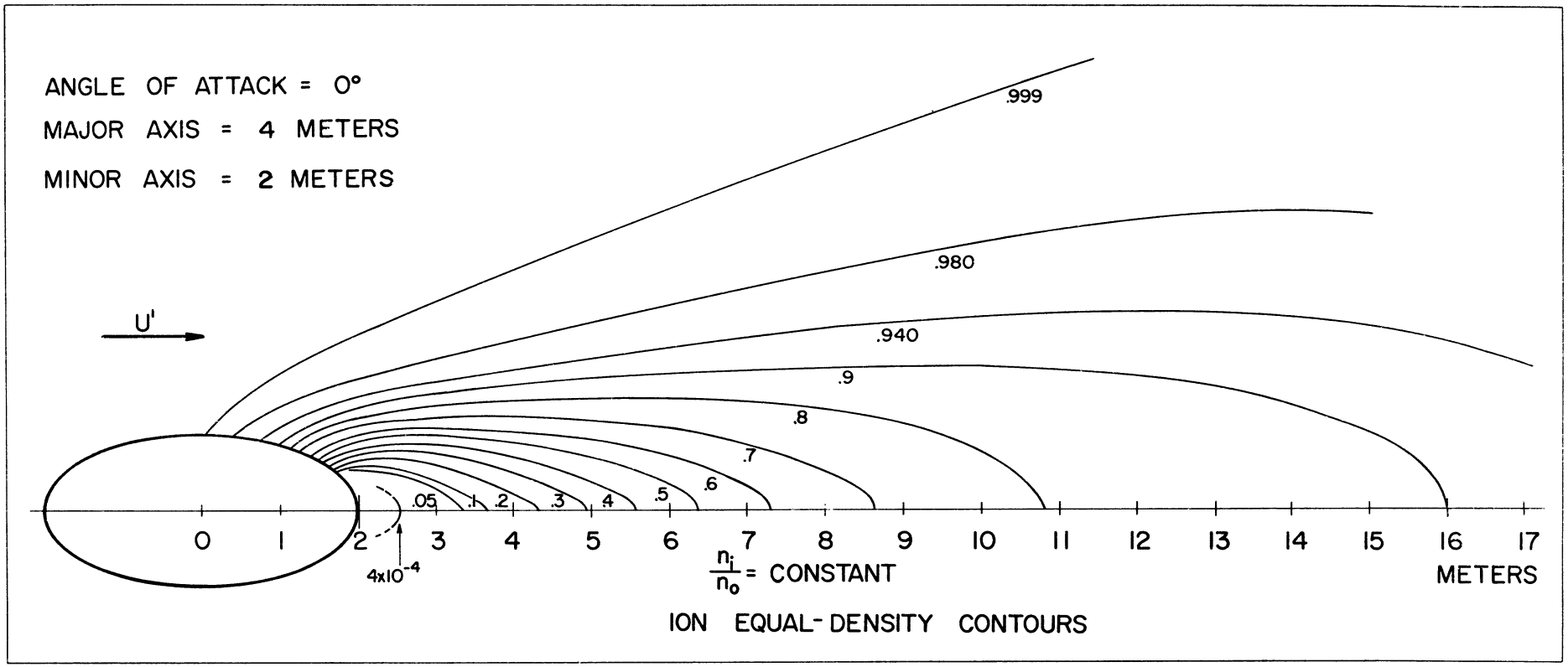
ANGLE OF ATTACK = 0°
MAJOR AXIS = 4 METERS
MINOR AXIS = 2 METERS
U'
.999
.980
.940
.9
.8
.7
.6
.5
.4
.3
.2
.1
.05
4x10⁻⁴
0 1 2 3 4 5 6 7 8 9 10 11 12 13 14 15 16 17
$\frac{n_i}{n_o}$ = CONSTANT
METERS
ION EQUAL-DENSITY CONTOURS

Figure 2.

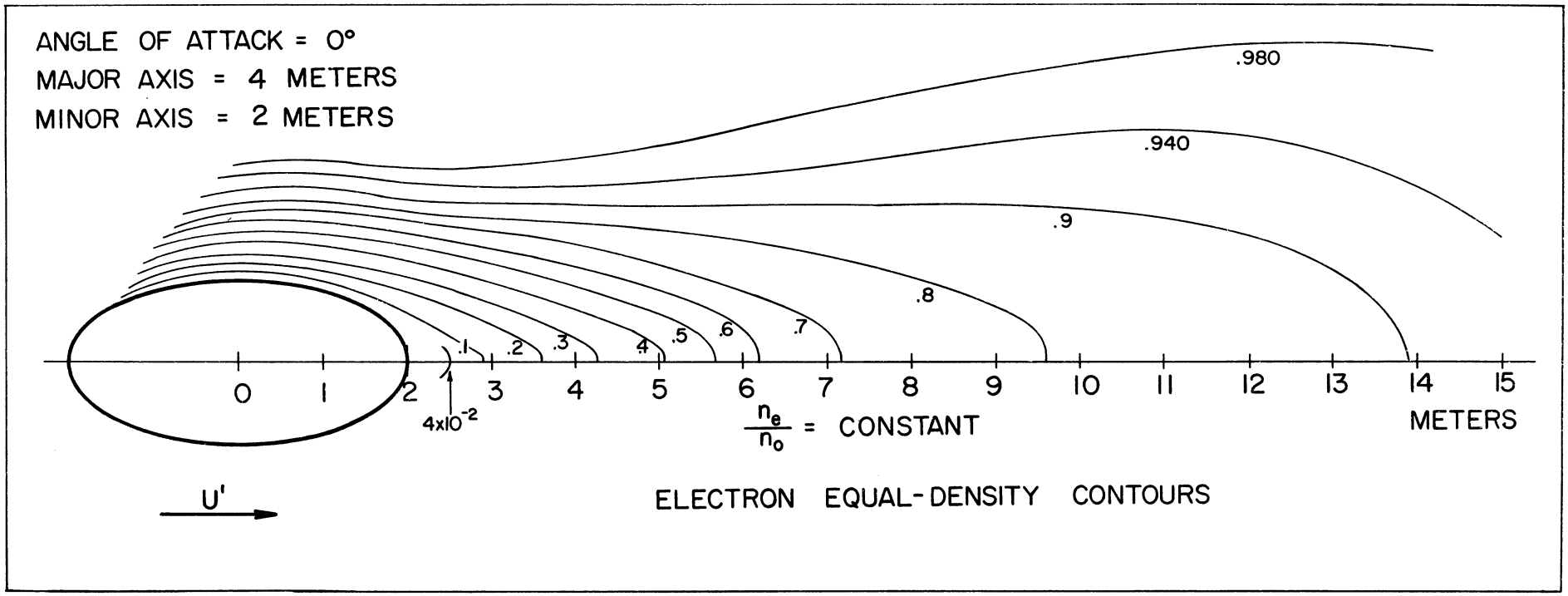
ANGLE OF ATTACK = 0°
MAJOR AXIS = 4 METERS
MINOR AXIS = 2 METERS
.980
.940
.9
.8
.7
.6
.5
.4
.3
.2
.1
0
1
2
3
4
5
6
7
8
9
10
11
12
13
14
15
4x10⁻²
n_e / n_o = CONSTANT
METERS
U'
ELECTRON EQUAL-DENSITY CONTOURS

Figure 3.

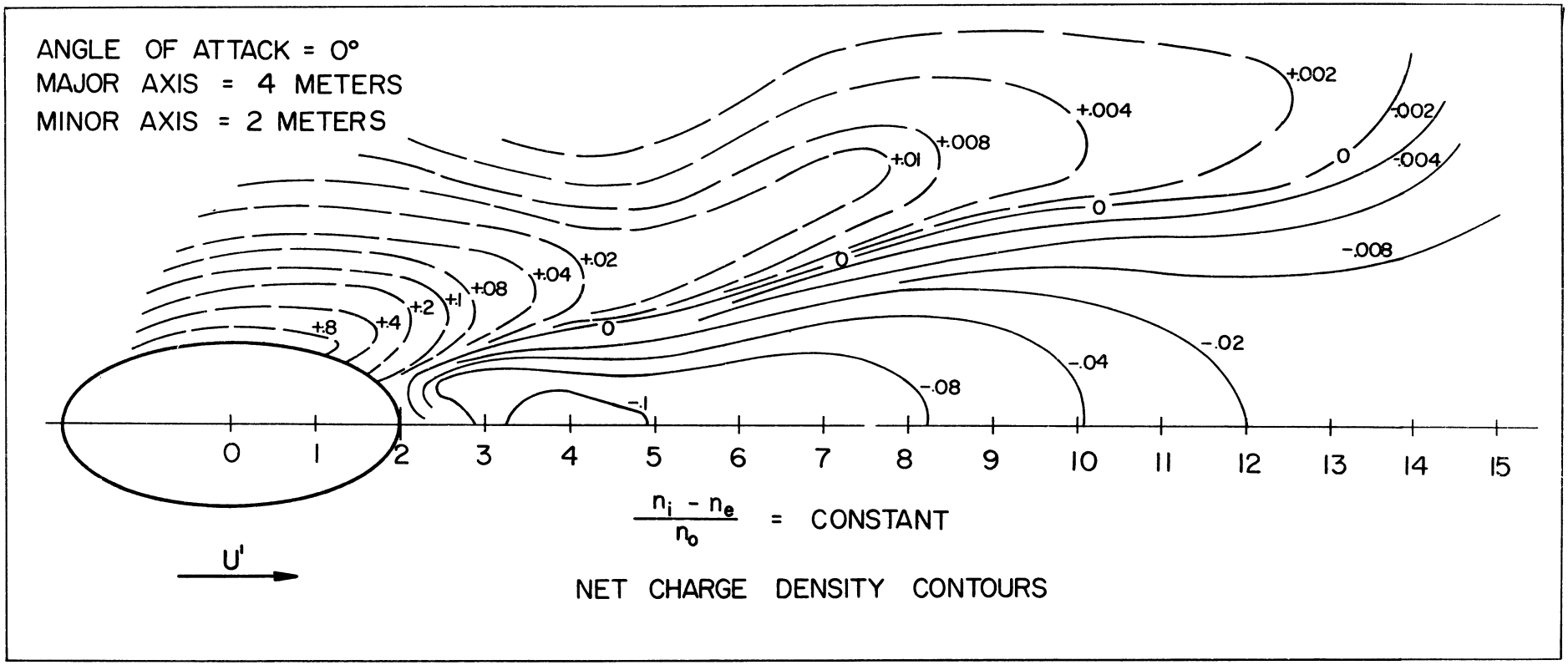
ANGLE OF ATTACK = 0°
MAJOR AXIS = 4 METERS
MINOR AXIS = 2 METERS
+.002
+.004
+.008
+.01
+.02
+.04
+.08
+.1
+.2
+.4
+.8
-.002
-.004
-.008
-.02
-.04
-.08
-.1
0
0 1 2 3 4 5 6 7 8 9 10 11 12 13 14 15
$\frac{n_i - n_e}{n_o}$ = CONSTANT
U'
NET CHARGE DENSITY CONTOURS

Figure 4.

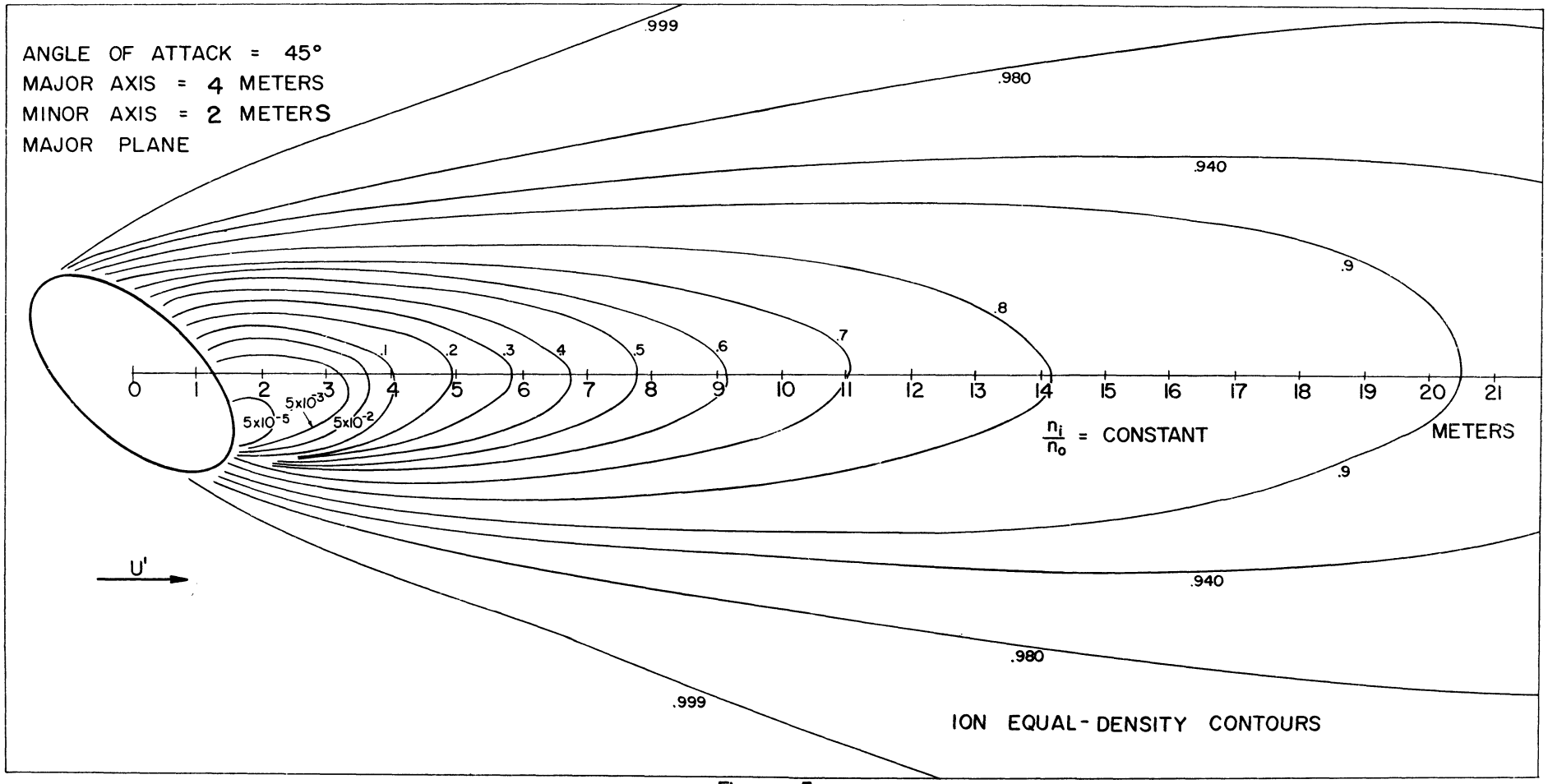
ANGLE OF ATTACK = 45°
MAJOR AXIS = 4 METERS
MINOR AXIS = 2 METERS
MAJOR PLANE
.999
.980
.940
.9
.8
.7
.6
.5
.4
.3
.2
.1
0 1 2 3 4 5 6 7 8 9 10 11 12 13 14 15 16 17 18 19 20 21
METERS
5x10-5
5x10-3
5x10-2
ni/no = CONSTANT
U'
ION EQUAL-DENSITY CONTOURS

Figure 5.

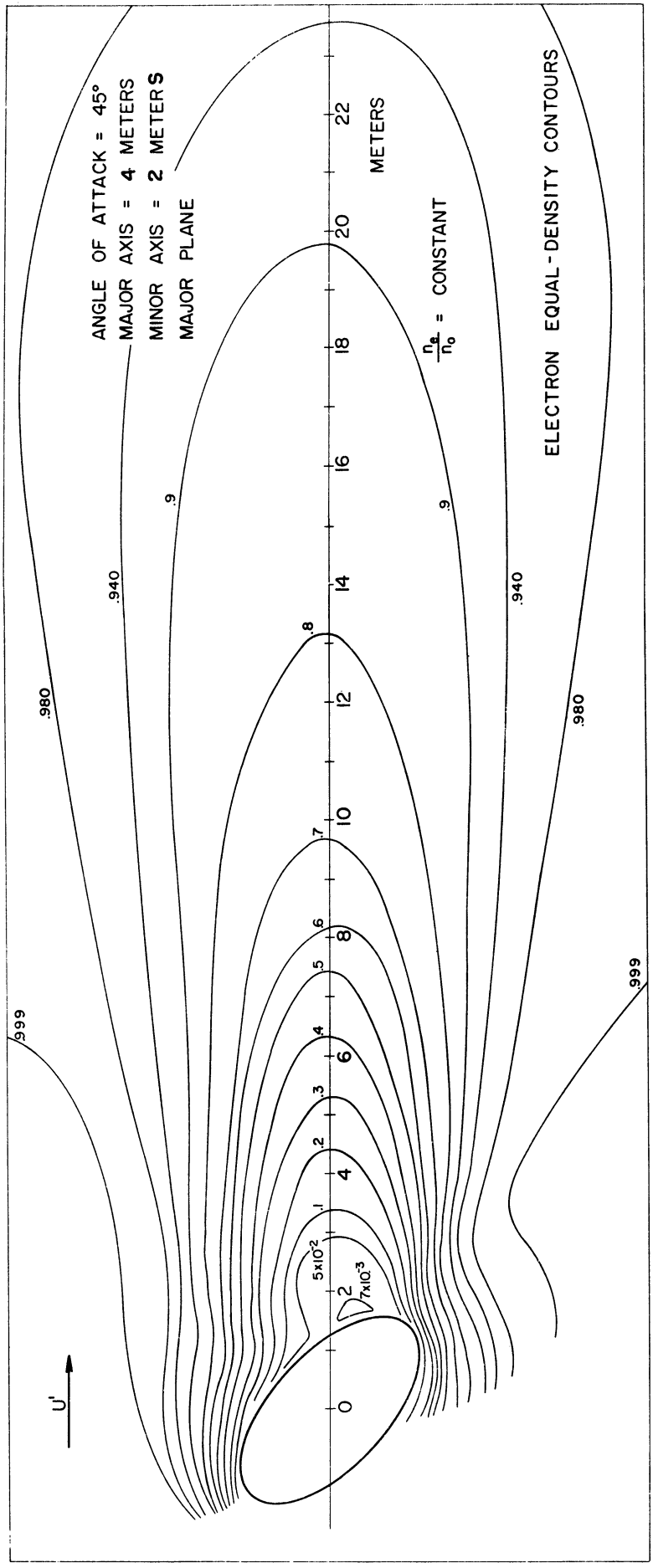
ELECTRON EQUAL-DENSITY CONTOURS
ANGLE OF ATTACK = 45°
MAJOR AXIS = 4 METERS
MINOR AXIS = 2 METERS
MAJOR PLANE
$\frac{n_e}{n_o}$ = CONSTANT
METERS
U'
.999
.980
.940
.9
.8
.7
.6
.5
.4
.3
.2
.1
5×10^{-2}
7×10^{-3}
0
2
4
6
8
10
12
14
16
18
20
22

Figure 6.

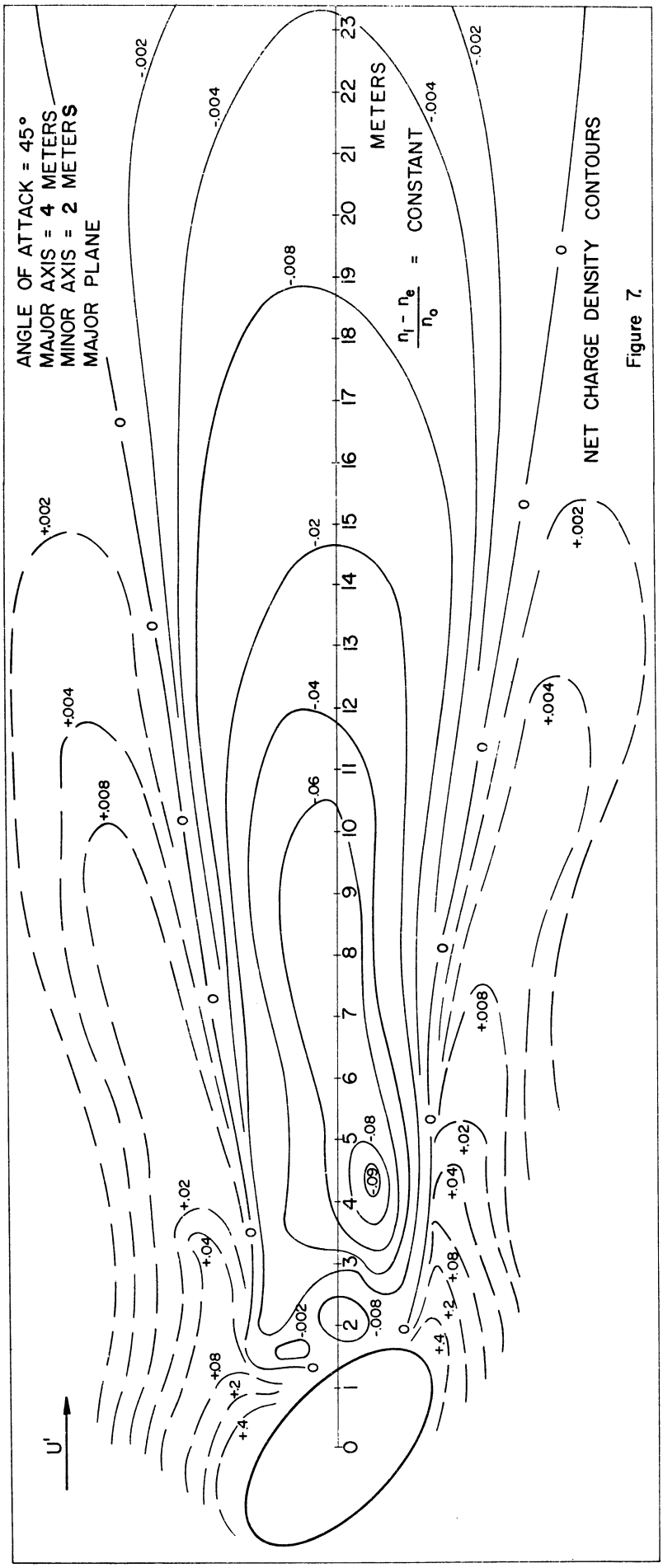
ANGLE OF ATTACK = 45°
MAJOR AXIS = 4 METERS
MINOR AXIS = 2 METERS
MAJOR PLANE
METERS
$\frac{n_i - n_e}{n_o}$ = CONSTANT
NET CHARGE DENSITY CONTOURS
U'

Figure 7.

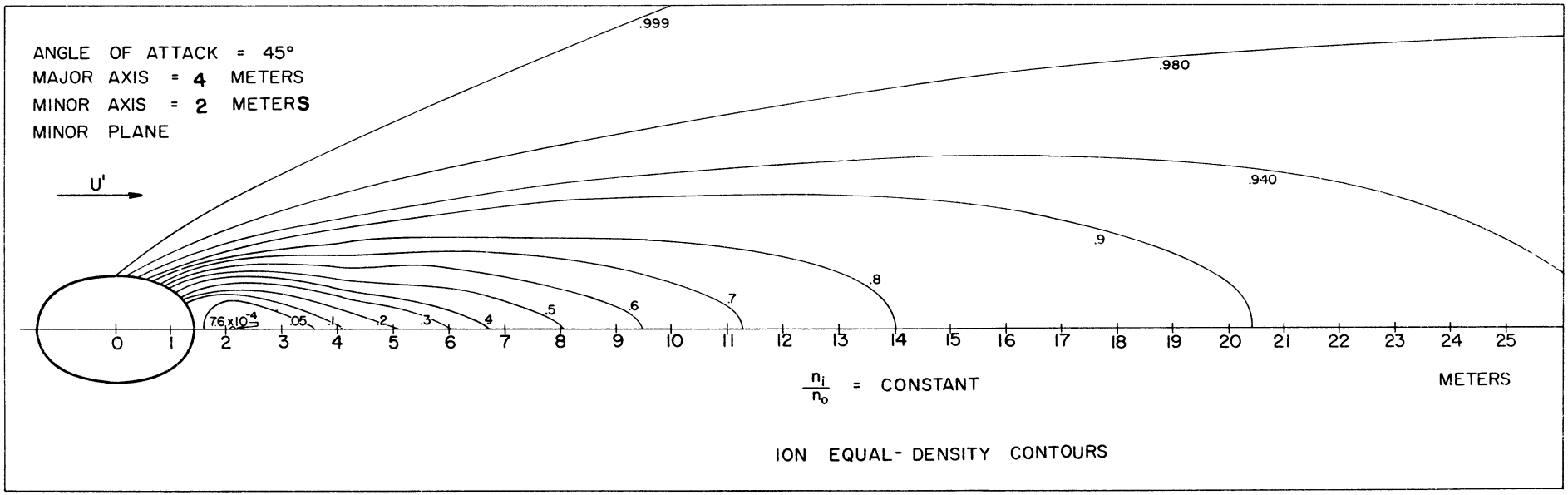
ANGLE OF ATTACK = 45°
MAJOR AXIS = 4 METERS
MINOR AXIS = 2 METERS
MINOR PLANE
U'
.999
.980
.940
.9
.8
.7
.6
.5
.4
.3
.2
.1
.05
7.6 x 10⁻⁴
0 1 2 3 4 5 6 7 8 9 10 11 12 13 14 15 16 17 18 19 20 21 22 23 24 25
METERS
$\frac{n_i}{n_o}$ = CONSTANT
ION EQUAL-DENSITY CONTOURS

Figure 8.

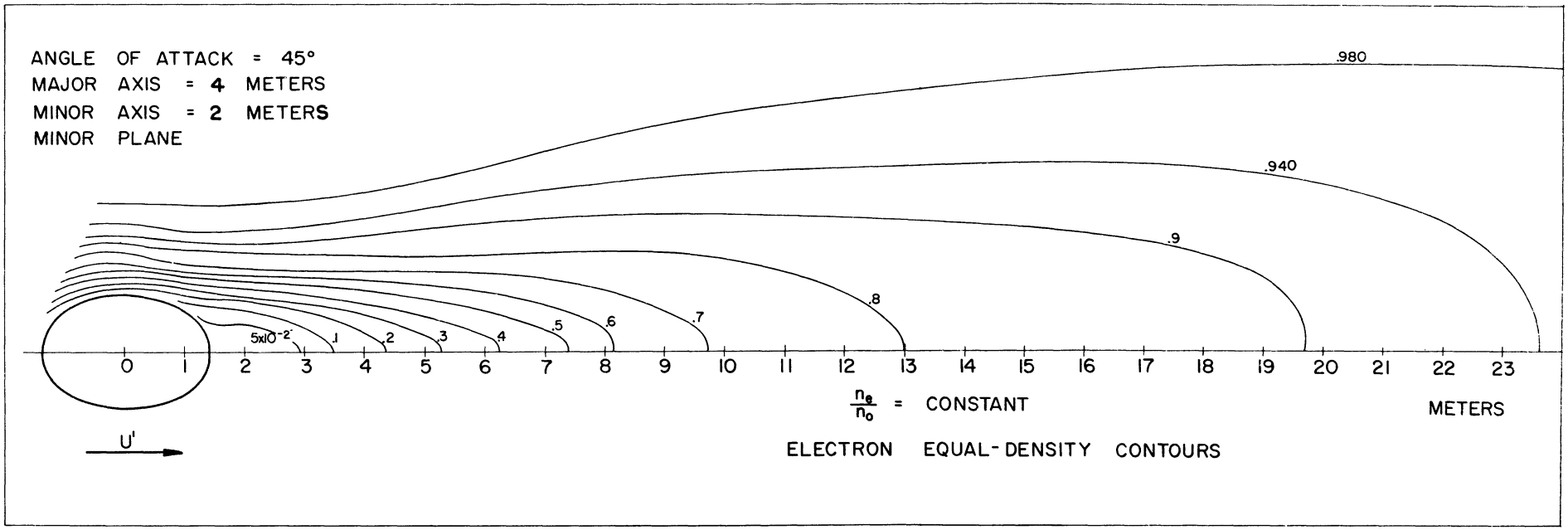
ANGLE OF ATTACK = 45°
MAJOR AXIS = 4 METERS
MINOR AXIS = 2 METERS
MINOR PLANE
.980
.940
.9
.8
.7
.6
.5
.4
.3
.2
.1
5x10⁻²
0 1 2 3 4 5 6 7 8 9 10 11 12 13 14 15 16 17 18 19 20 21 22 23
METERS
U'
$\frac{n_e}{n_o}$ = CONSTANT
ELECTRON EQUAL-DENSITY CONTOURS

Figure 9.

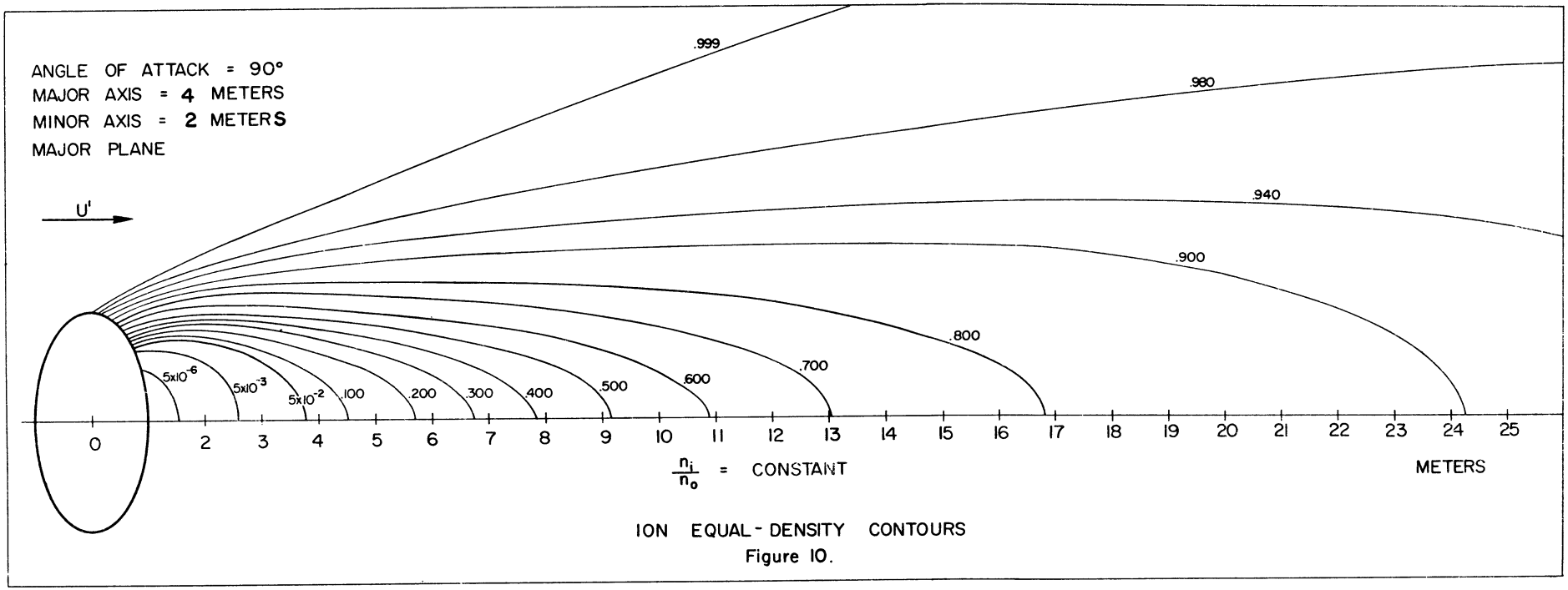

ION EQUAL-DENSITY CONTOURS
Figure 10.

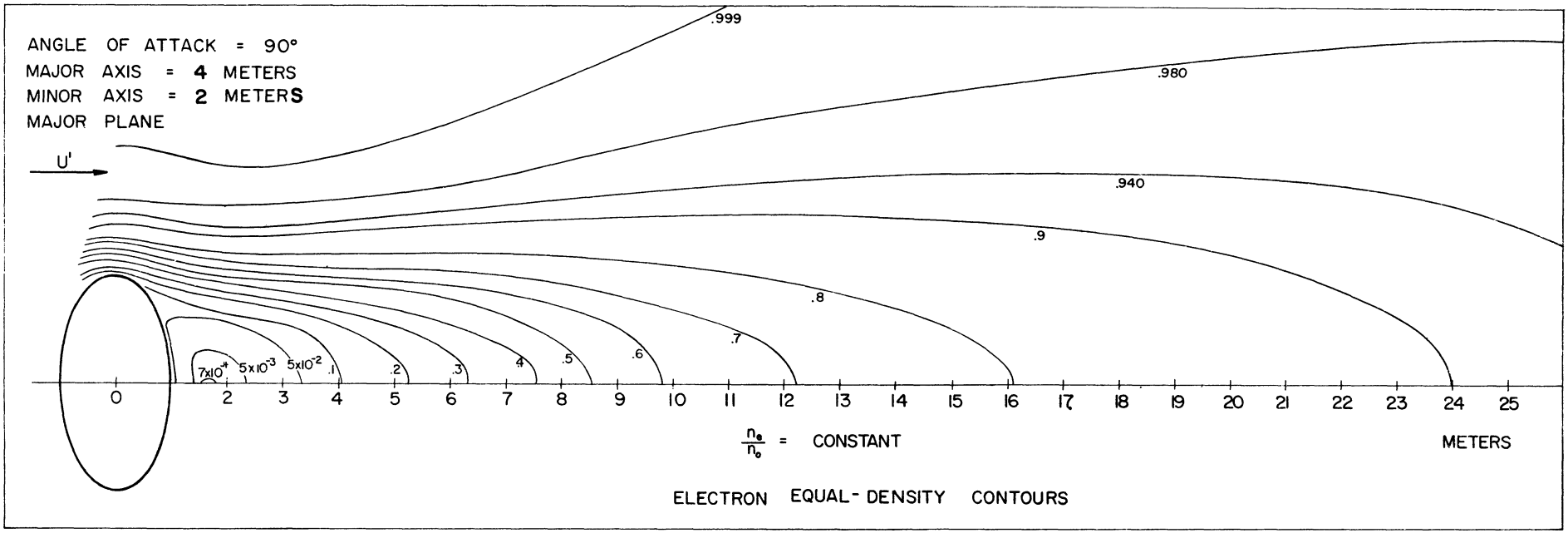
ANGLE OF ATTACK = 90°
MAJOR AXIS = 4 METERS
MINOR AXIS = 2 METERS
MAJOR PLANE
U'
.999
.980
.940
.9
.8
.7
.6
.5
.4
.3
.2
.1
7x10⁻⁴
5x10⁻³
5x10⁻²
0 2 3 4 5 6 7 8 9 10 11 12 13 14 15 16 17 18 19 20 21 22 23 24 25
METERS
$\frac{n_e}{n_o}$ = CONSTANT
ELECTRON EQUAL-DENSITY CONTOURS

Figure 11.

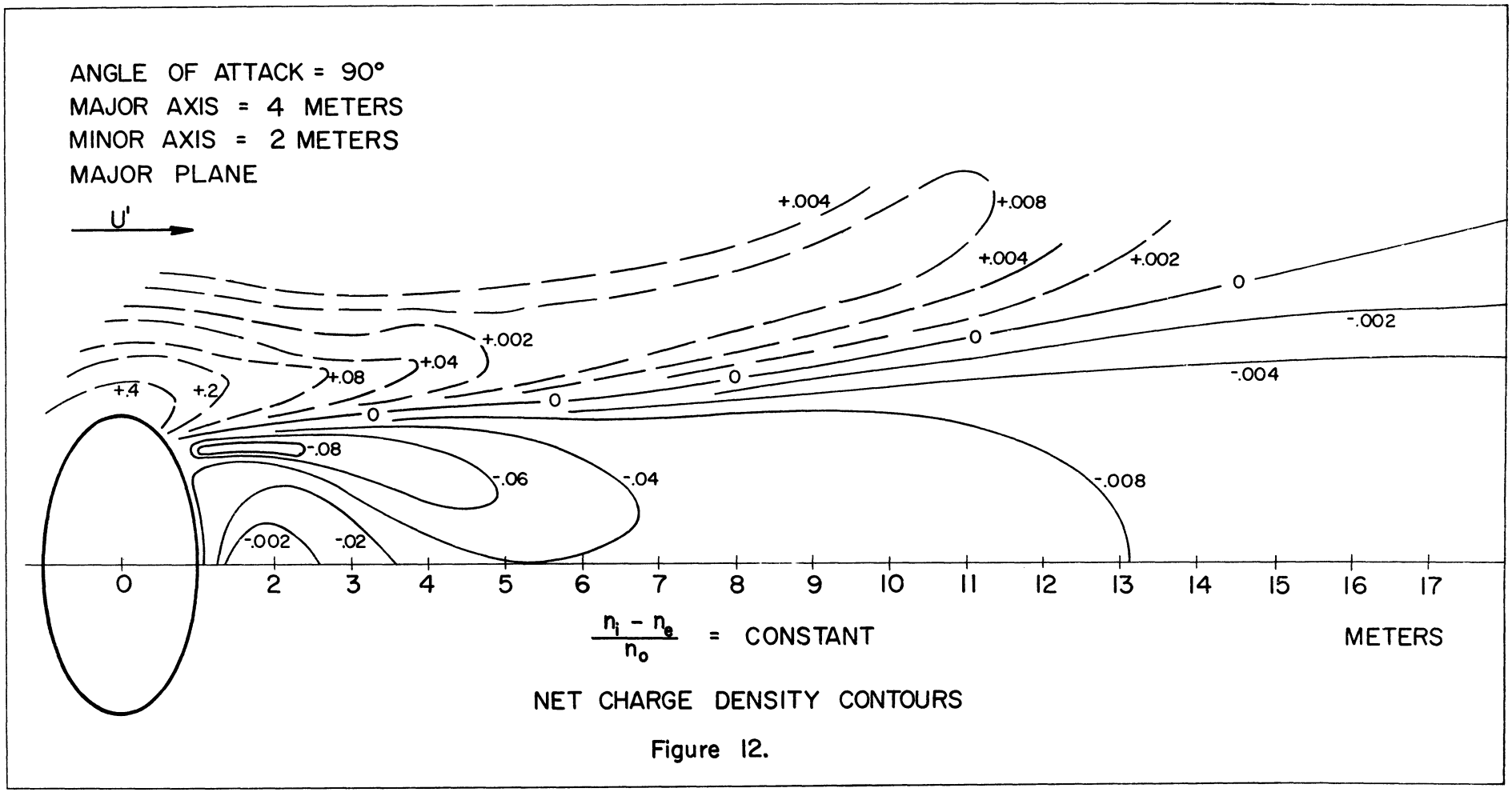

NET CHARGE DENSITY CONTOURS

Figure 12.

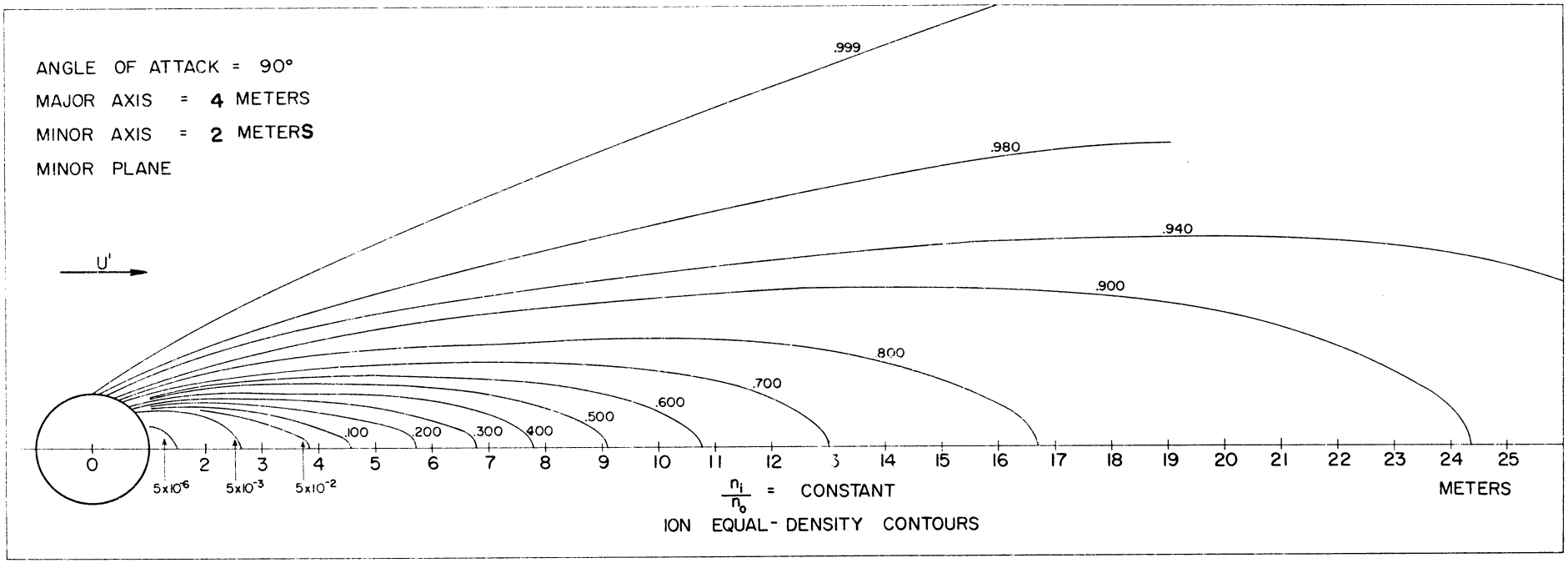
ANGLE OF ATTACK = 90°
MAJOR AXIS = 4 METERS
MINOR AXIS = 2 METERS
MINOR PLANE
U'
.999
.980
.940
.900
.800
.700
.600
.500
.400
.300
.200
.100
0
2
3
4
5
6
7
8
9
10
11
12
3
14
15
16
17
18
19
20
21
22
23
24
25
5x10⁻⁶
5x10⁻³
5x10⁻²
METERS
ni/no = CONSTANT
ION EQUAL-DENSITY CONTOURS

Figure 13.

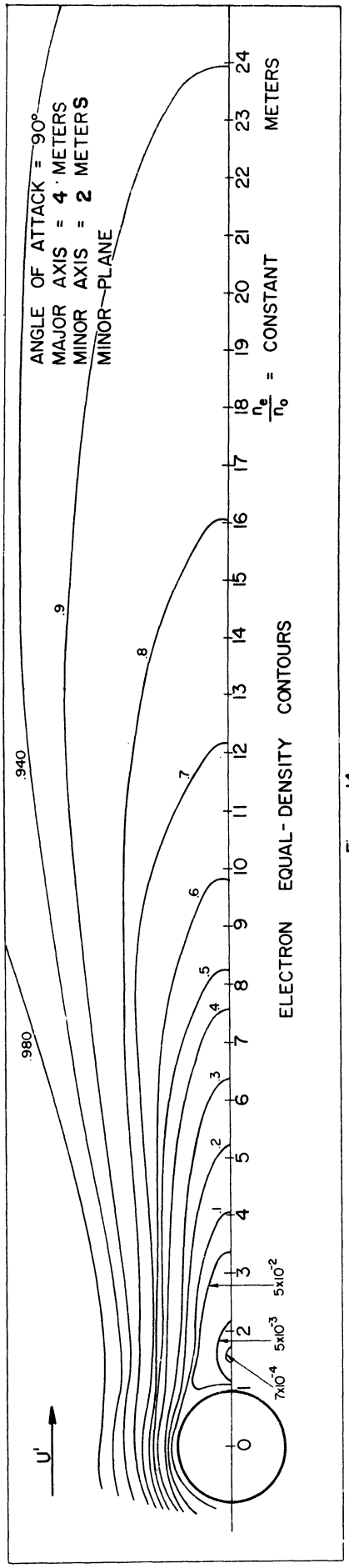
ANGLE OF ATTACK = 90°
MAJOR AXIS = 4 METERS
MINOR AXIS = 2 METERS
MINOR-PLANE
ELECTRON EQUAL-DENSITY CONTOURS
$\frac{n_e}{n_0}$ = CONSTANT
METERS
U'
.980
.940
.9
.8
.7
.6
.5
.4
.3
.2
.1
7×10^{-4}
5×10^{-3}
5×10^{-2}

Figure 14.